Acta Crystallographica Section F
Structural Biology and Crystallization Communications
ISSN 1744-3091

Crystallization and preliminary X-ray crystallographic analysis of sterol transcription factor Upc2 from *Saccharomyces cerevisiae*

Subin Ha,[a] Junsen Tong,[a] Huiseon Yang,[a] Hyung-Seop Youn,[b] Soo Hyun Eom[b] and Young Jun Im[a]*

[a]College of Pharmacy, Chonnam National University, Gwangju 500-757, Republic of Korea, and [b]Department of Life Science, Gwangju Institute of Science and Technology, Gwangju 500-712, Republic of Korea

Correspondence e-mail: imyoungjun@jnu.ac.kr

Received 5 October 2012
Accepted 21 December 2012

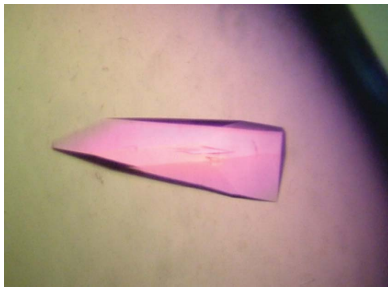

Upc2, a zinc-cluster transcription factor, is a regulator of ergosterol biosynthesis in yeast. In response to sterol levels, the transcriptional activity of Upc2 is controlled by the C-terminal domain. In this study, the C-terminal regulatory domain of Upc2 from *Saccharomyces cerevisiae* was purified and crystallized by the vapour-diffusion method. To improve the diffraction quality of Upc2 crystals, a Upc2 fusion protein in which 11 residues of the variable loop (residues 715–725) were replaced by T4 lysozymes in Upc2 (Upc2-T4L) was engineered. The Upc2-T4L crystals diffracted to 2.9 Å resolution using synchrotron radiation. The crystal was trigonal, belonging to space group $P3_2$ with unit-cell parameters a = 67.2, b = 67.2, c = 257.5 Å. The Matthews coefficient was determined to be 3.41 Å^3 Da^{-1} with two molecules in the asymmetric unit. Initial attempts to solve the structure by the single-anomalous dispersion technique using selenomethionine were successful.

1. Introduction

Ergosterol is the major fungal membrane sterol that regulates membrane fluidity, plasma membrane biogenesis and function (Zhang & Rao, 2010). Ergosterol homeostasis is critical for fungal cells. Genes encoding biosynthetic enzymes of ergosterol are partly regulated at the transcriptional level. In *Saccharomyces cerevisiae*, two transcriptional factors, Upc2 and Ecm22, have been implicated in ergosterol regulation by binding to the promoters of most ergosterol biosynthetic (ERG) genes and activating transcription upon sterol depletion (Vik & Rine, 2001). Upc2 and Ecm22 are about 900 amino acids in length and share a high level of sequence similarity in the N-terminal DNA-binding domains (57% sequence identity in residues 1–100 between Upc2 and Ecm22) characterized by a conserved zinc(II)$_2$Cys$_6$ zinc-finger motif (Davies *et al.*, 2005). The C-terminal conserved region of about 300 amino-acid residues (75% identity) contains a transcription activation domain. It was suggested that the C-terminal transcription activation domains of both Upc2 and Ecm22 are targeted by a repressor protein or small molecules that mask their intrinsic activation capabilities (Davies *et al.*, 2005). The conserved N-terminal DNA-binding domain and the C-terminal regulatory domain (CRD) are connected by highly dissimilar middle regions that are rich in glutamine and asparagine.

The human pathogen *Candida albicans* is responsible for a large proportion of infections in immunocompromised individuals and the emergence of drug-resistant strains is of medical concern. Upc2 of *C. albicans* regulates *ERG11* which encodes the target of azole drugs including fluconazole and ketoconazole. Resistance to azole drugs is partly due to alteration of the ergosterol biosynthetic pathway. Gain-of-function mutations in Upc2 that contribute to drug resistance have been identified in clinical isolates (Dunkel *et al.*, 2008). Mutations in the C-terminal regulatory domain of Upc2 (A643V, A643T or G648D) result in constitutive activation of the transcription factor. This leads to an increased expression of Erg11 which contributes to decreased susceptibility of the strains to azoles (Hoot *et al.*, 2011; Heilmann *et al.*, 2010). Yeast normally does not take up sterols from the environment under aerobic conditions. A gain-of-function mutation (G888D) in the C-terminal domain of *UPC2*, designated as *upc2-1*, results in constitutive activation of the transcription factor and allows a high level of aerobic sterol uptake in *S. cerevisiae* (Lewis

et al., 1988; Valachovic *et al.*, 2006). These mutations are in close proximity to the C-terminal portion of the protein, which may indicate that the CRD is important in the regulation of its functional activity (Hoot *et al.*, 2011). Deletion of *UPC2* in *C. albicans* leads to decreased tolerance to azole drugs and deletion of both *UPC2* and *ECM22* in *S. cerevisiae* is lethal in certain yeast strains (Shianna *et al.*, 2001).

The CRDs of Upc2 and Ecm22 have no recognizable similarity to any characterized protein domains and have no homology to proteins of known structure in the Protein Data Bank. However, conservation of this region across fungal species and previous functional studies indicate that the CRD may represent a discrete domain. Consistently, the CRD is predicted to have a secondary structure consisting of 13 α-helices, indicating the presence of a globular domain in this region. Although Upc2 responds to sterol levels in the cell, whether sterol molecules are direct ligands of Upc2 is not known. In order to obtain a structural insight into the regulatory mechanism of Upc2, we initiated crystallographic studies of Upc2 CRD. Here, we report the crystallization and X-ray data collection of Upc2 CRD from *S. cerevisiae*.

2. Materials and methods

2.1. Cloning and protein expression

DNA encoding the C-terminal regulatory domain (residues 598–913) of Upc2 (UniProt ID Q12151) was amplified by polymerase chain reaction (PCR) using *S. cerevisiae* genomic DNA as a template. The gene for Upc2 spanning residues 598–913 was amplified using the oligonucleotide primers 5′-GTAATATCATATGGATCTTTCTAC-CAAAGGC-3′ (forward) and 5′-GTATAATCTCGAGTCATAAC-GAAAAATCAGAG-3′ (reverse). For the PCR amplification of Upc2 spanning residues 598–878, the following reverse primer was used: 5′-GTATAATCTCGAGTCATTGAGGCAGCACCTGCG-3′.

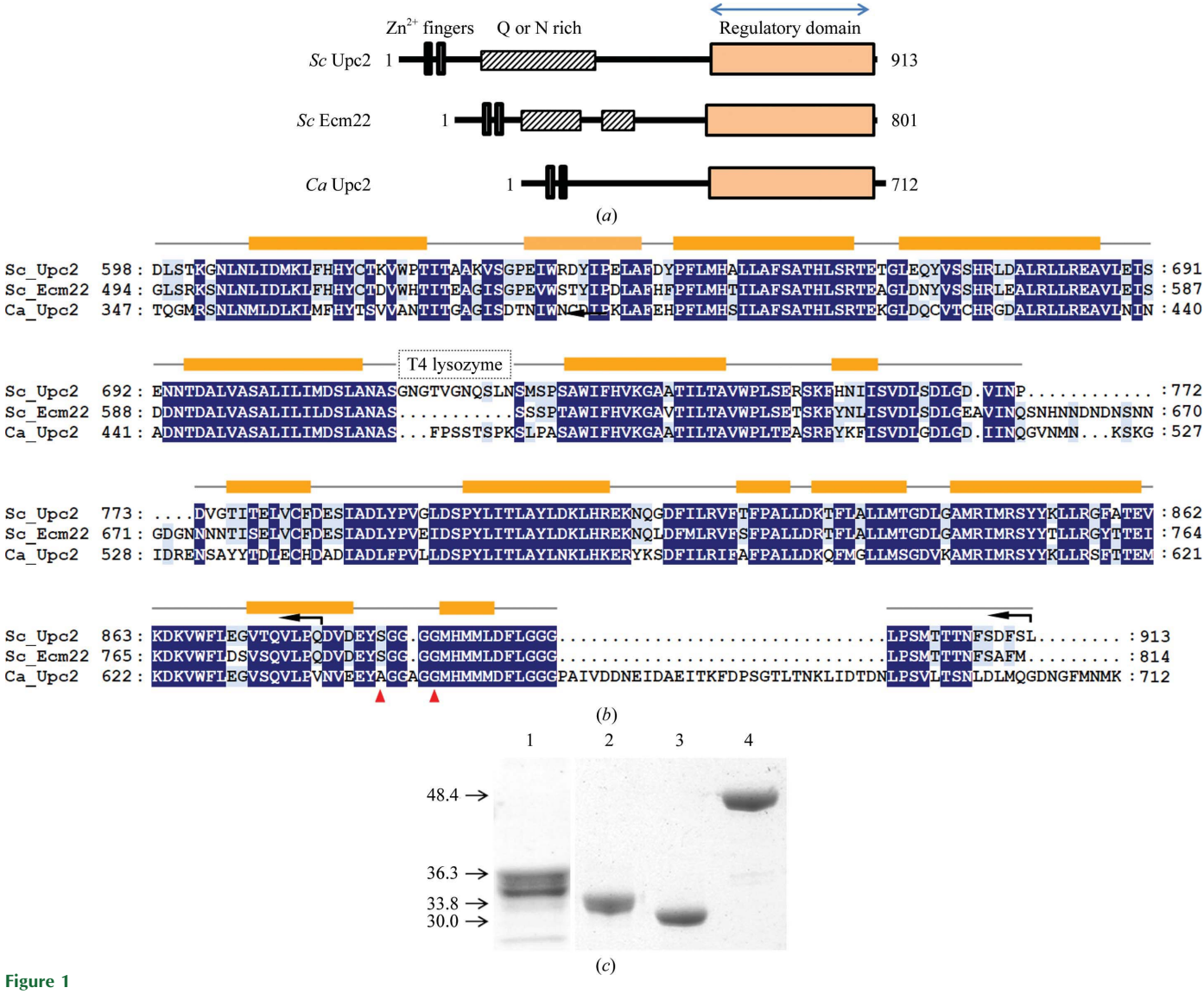

Figure 1
(*a*) Schematic domain representation of Upc2 and Ecm22. (*b*) Sequence alignment of Upc2 homologues. The C-terminal regulatory domains of Upc2 and Ecm22 from *S. cerevisiae* and Upc2 from *C. albicans* were used for the alignment. Secondary-structure elements of α-helices for *S. cerevisiae* Upc2 are indicated by rectangles. Secondary structures were predicted by the *PredictProtein* server (http://www.predictprotein.org/). Gain-of-function mutation sites are indicated by red triangles. (*c*) Purified Upc2 constructs used for crystallization studies. Lane 1, Upc2-CRD (residues 585–913); lane 2, Upc2-CRD (residues 598–913, Δ715–725); lane 3, Upc2-CRD (residues 598–878) with the loop deletion (residues 715–725); lane 4, Upc2-CRD (residues 598–878) with T4 lysozyme fusion in the loop (residues 715–725). Molecular masses are labelled in kDa.

The PCR products were subcloned into the *Nde*I and *Xho*I sites of a pET-28b vector (Novagen). Upc2 was tagged with an N-terminal hexahistidine followed by a thrombin protease cleavage site (LVPR/GS). All mutations were carried out using pET28b-*Upc2* as a template and appropriate primers based on the protocol of the QuikChange site-directed mutagenesis kit (Stratagene). Open reading frames of all mutant genes were confirmed by DNA sequencing. The variable region (residues 715–725) in Upc2 was replaced by a dipeptide sequence (Val–Asp) of the *Sal*I restriction enzyme recognition sequence by PCR-based mutagenesis (Fig. 1). After this, DNA encoding T4 lysozyme (residues 2–161) with *Sal*I restriction enzyme sites in 5′ and 3′ overhangs was inserted into the *Sal*I site of pET28b-*Upc2*. The Upc2-T4L construct used for structure determination had the following amino-acid sequence: GSHM (from the multiple cloning site)–Upc2 (residues 598–714)–VD (*Sal*I enzyme site)–T4 lysozyme (residues 2–161)–VD (*Sal*I enzyme site)–Upc2 (residues 726–878). The pET28b-*Upc2-T4L* (residues 598–878, 715–725Δ::*T4L*) was transferred into *Escherichia coli* strain BL21 Star (DE3) cells (Invitrogen). Transformed cells were grown to an OD_{600} of 0.8 at 310 K in Luria–Bertani (LB) medium and protein expression was induced by the addition of 0.5 m*M* isopropyl *β*-D-1-thiogalactopyranoside (IPTG). The culture was incubated for a further 12 h at 293 K before harvesting cells. To prepare selenomethionyl Upc2-T4L protein for phase determination, the methionine-pathway inhibition technique was exploited using a heterotrophic *E. coli* strain (Doublié, 1997). A 5 ml overnight culture of *E. coli* BL21 Star (DE3) cells harbouring pET28b-*Upc2-T4L* in LB medium was directly inoculated into an 800 ml culture of a minimal medium supplemented with 50 mg l^{-1} L-selenomethionine. The culture was incubated at 310 K until the OD_{600} reached 0.8. Protein expression was induced by the addition of 0.5 m*M* IPTG and cultures were incubated at 293 K for a further 24 h.

2.2. Protein purification

Cells expressing Upc2-T4L were resuspended in lysis buffer (2× PBS buffer supplemented with 20 m*M* imidazole) and lysed by sonication. Crude cell lysates were clarified by centrifugation at 13 000*g* for 45 min. The supernatant containing His-Upc2-T4L was applied to an Ni–NTA affinity column (GE Healthcare). The Ni–NTA column was thoroughly washed with the lysis buffer. The fusion protein was eluted from the column using 0.1 *M* Tris–HCl pH 7.5, 0.3 *M* imidazole, 0.3 *M* NaCl. The eluate was concentrated to 10 mg ml^{-1} and the His tag was removed by cleavage with thrombin protease. Upc2-T4L was subjected to size-exclusion chromatography on a Superdex 200 column (GE Healthcare) equilibrated with 20 m*M* Tris–HCl pH 8.0, 0.3 *M* NaCl. The peak fractions containing Upc2-T4L were concentrated to 10 mg ml^{-1} for crystallization. Typically, we purified 10 mg soluble Upc2-T4L from a litre of culture. Purification of selenomethionyl Upc2-T4L and other Upc2 constructs essentially followed the same procedure as described above.

2.3. Crystallization of Upc2-T4L

Preliminary crystallization experiments were carried out at 295 K using customized crystallization screening solutions by vapour-diffusion methods. 0.8 µl protein solution and 0.8 µl precipitant solution were dispensed using a multichannel pipette on 96-well crystallization plates. Crystals of Upc2 CRD (residues 598–913, Δ715–725) were grown in 0.1 *M* MES pH 6.0, 12.5% polyethylene glycol (PEG) 6000, 0.2 *M* Li_2SO_4 with a typical size of 0.01 mm in length (Fig. 2*a*). Crystals of the truncated Upc2 CRD (residues 598–878, Δ715–725) lacking the C-terminal region (residues 879–913) were grown to typical dimensions of 0.02 × 0.1 × 0.1 mm in 0.1 *M* HEPES pH 7.0, 15% PEG 8000, 0.1 *M* sodium citrate (Fig. 2*b*). However, optimization of the crystallization conditions to obtain diffracting crystals was not successful. Initial crystals of Upc2 CRD-T4L (residues 598–878, 715–725Δ::*T4L*) in 96-well crystallization plates appeared after 1 d using a solution consisting of 0.1 *M* HEPES pH 7.0, 15%(*w*/*v*) PEG 8000, 0.2 *M* sodium citrate. Subsequent crystallization experiments were carried out using 15-well screw-cap plates (Qiagen) by the hanging-drop vapour-diffusion method. Owing to crystal damage upon transfer to cryosolutions, the crystallization condition was further optimized in order to obtain crystals suitable for cryoprotection. A drop consisting of 2 µl protein solution was mixed with 2 µl precipitant solution and equilibrated against 1 ml reservoir solution consisting of 0.1 *M* HEPES pH 7.0, 10.0–12.5%(*w*/*v*) PEG 8000, 0.2 *M* sodium citrate, 7.5% glycerol. Selenomethionine-labelled crystals were typically grown to maximum dimensions of 0.15–0.30 mm in 2 weeks by microseeding techniques using native crystals (Fig. 2*c*).

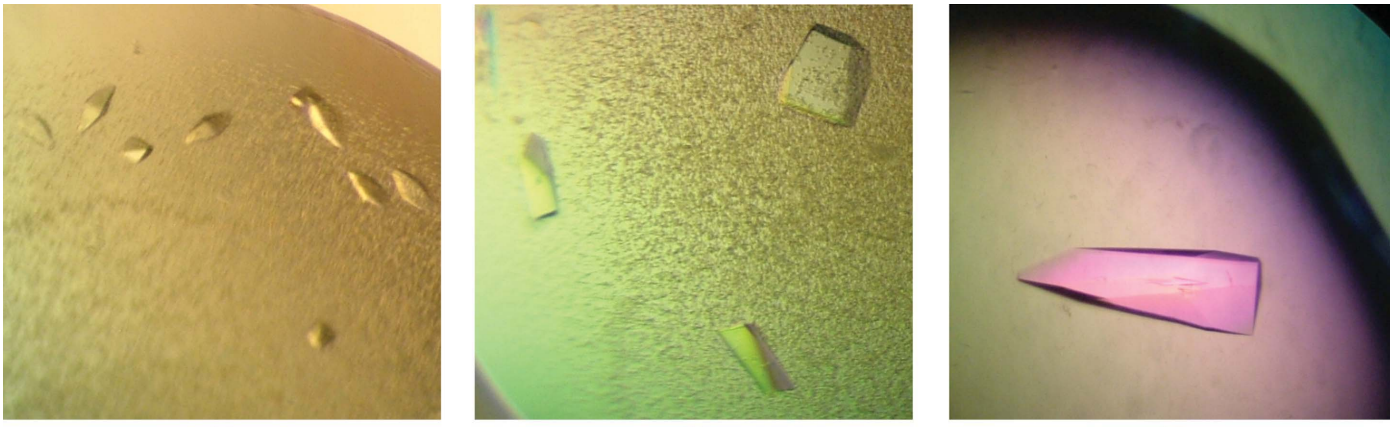

(*a*) (*b*) (*c*)

Figure 2
Crystals of Upc2 CRD from *S. cerevisiae*. (*a*) Crystals of Upc2 CRD (residues 598–913, Δ715–725) grown in 0.1 *M* MES pH 6.0, 12.5% PEG 6000, 0.2 *M* Li_2SO_4 with typical dimensions of 0.02 × 0.01 × 0.01 mm. (*b*) Native crystals of Upc2 CRD (residues 598–878, Δ715–725) were grown in 0.1 *M* HEPES pH 7.0, 15% PEG 8000, 0.1 *M* sodium citrate with typical dimensions of 0.02 × 0.1 × 0.1 mm. (*c*) A selenomethionine-labelled Upc2-T4L crystal with dimensions of 0.1 × 0.15 × 0.3 mm was grown in 0.1 *M* HEPES pH 7.0, 10% PEG 8000, 0.1 *M* sodium citrate, 7.5% glycerol by microseeding techniques.

2.4. Diffraction experiment

The crystals were cryoprotected by transferring them into reservoir solution supplemented with an additional 10%(*v*/*v*) glycerol and were flash-cooled by immersion in liquid nitrogen. The crystals were preserved in a cryogenic N_2-gas stream (∼100 K) during diffraction experiments. Diffraction data for the selenomethionine-labelled crystals were collected at a peak wavelength of 0.97921 Å using an ADSC Q210 CCD detector on the AR-NW12A beamline at the Photon Factory, Japan. All data were processed and scaled using *HKL*-2000 (Otwinowski & Minor, 1997) and handled with the *CCP*4 program suite (Winn *et al.*, 2011). SAD phasing was performed with the program *SOLVE* (Terwilliger & Berendzen, 1999) and density modification was performed using *RESOLVE* (Terwilliger, 2000).

3. Results and discussion

Upc2 CRD was cloned into the vector providing N-terminal hexahistidine affinity tags. The fusion protein was expressed in *E. coli* BL21(DE3) Star cells. The intact regulatory domain (residues 598–913) underwent proteolytic fragmentation by endogenous bacterial proteases during the expression and purification steps. This construct did not yield crystals in initial crystallization trials, possibly owing to the presence of flexible loop regions. Residues 715–725 and the C-terminal glycine-rich region were predicted to be disordered by secondary-structure prediction (http://www.predictprotein.org/). Therefore, the variable loop (residues 715–725) and the C-terminal flexible loop (residues 879–913) were deleted stepwise to obtain stable constructs (Fig. 1*c*). The construct with a deletion in the variable loop yielded small crystals with poor morphology in 0.1 *M* MES pH 6.0, 12.5% PEG 6000, 0.2 *M* Li_2SO_4 (Fig. 2*a*). Additional deletion of the C-terminal 35 residues (residues 879–913) yielded crystals with improved quality which diffracted to 7 Å resolution with synchrotron radiation (Figs. 2*b* and 3). To improve the diffraction quality of the crystals, surface-entropy reduction (SER) and truncation of the constructs were tested. Seven residues (K619A, K628S, R636A, E692A-N693A, R752A, E812A-K813A and K853S) were selected for the SER approach based on surface-entropy reduction prediction (http://services.mbi.ucla.edu/SER) and by manual selection on glutamate or lysine residues on α-helices. R752A and E692A-N693A mutants resulted in a slight improvement in crystallization properties with faster nucleation and an increase in crystal size. However, the diffraction limit was not improved by the mutations. K619A, E812A-K813A and K853S mutants did not yield any crystals. The other two mutations (K628S and R636A) had no apparent improvement in crystallization properties and diffraction limits.

Therefore, we applied the T4 lysozyme-fusion technique, which was successfully exploited in the crystallization of several GPCR receptors, to a flexible loop to enhance the crystallization and diffraction quality (Rosenbaum *et al.*, 2007; Chien *et al.*, 2010). The replacement of an internal flexible loop by a globular domain might be advantageous in crystallization by providing new rigid lattice contacts. The internal lysozyme fusion is expected to have lower entropy in the hinge movement between domains than fusing the lysozyme to the N- or C-termini of a target protein. Upc2 homologues including Ecm22 in *S. cerevisiae* and *C. albicans* have variable insertions or deletions in residues 714–725 and 772–775 (Fig. 1*c*) which might be good sites for T4L insertion. We tested T4 lysozyme replacements in the loop region (residues 715–725) with several different lengths of linkers (VD or VDST for the N-terminus of lysozyme and VD or STVD for the C-terminus of lysozyme). The fusion constructs with four different lengths of linkers were expressed and purified. Only the T4 lysozyme fusions with the shortest two amino-acid linkers, Val–Asp, in both the N- and C-termini of the lysozyme yielded diffracting crystals with good morphology (Fig. 2*c*). Another lysozyme replacement in residues 722–778 of Upc2 and the

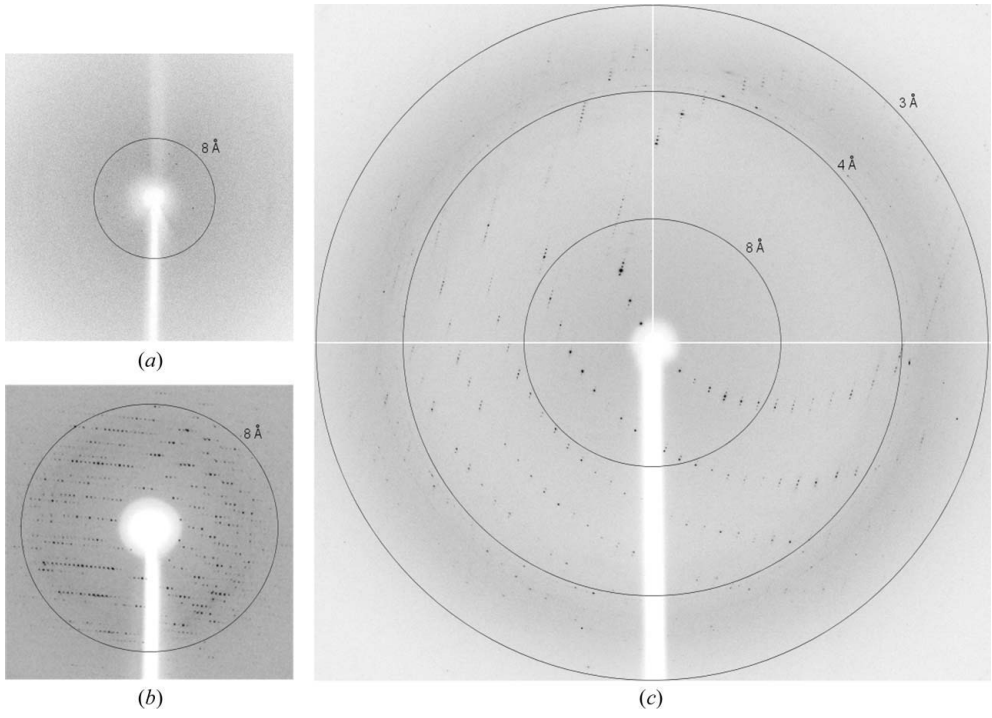

Figure 3
Diffraction images of Upc2 crystals. (*a*) A diffraction image of a Upc2 CRD crystal (residues 598–913, Δ715–725). (*b*) A diffraction image of a Upc2 CRD (residues 598–878, Δ715–725) crystal; the image was magnified 2.5 times at the beam centre. (*c*) A typical diffraction image of selenomethionine-labelled Upc2 T4L crystals. Images were collected from a single cryocooled crystal with a crystal-to-detector distance of 310 mm using a wavelength of 0.97921 Å. The edges of the detector show a d_{min} of 3.0 Å.

Table 1
Summary of diffraction data statistics for SeMet Upc2-T4L.

Values in parentheses are for the highest resolution shell.

Construct	Upc2-T4L [residues 598–878, 715–725Δ::*T4L*]
Wavelength (Å)	0.97921
X-ray source	AR-NW12A, Photon Factory
Space group	$P3_2$
Oscillation angle per image (°)	0.5
Rotation range (°)	360
Unit-cell parameters (Å)	a = 67.2, b = 67.2, c = 257.5
Resolution (Å)	50–2.9 (3.06–2.90)
Observed No. of reflections	225954 (28174)
No. of unique reflections	28788 (4194)
Multiplicity	7.8 (6.7)
$\langle I/\sigma(I)\rangle$	12.8 (3.7)
$R_{\rm merge}$† (%)	9.4 (35.8)
Data completeness (%)	99.8 (99.0)
Wilson B factor (Å^2)	80.2
Phasing	SeMet SAD
$R_{\rm anom}$ (50–3 Å)	0.069
Figure of merit	0.44 [*SOLVE*], 0.70 [*RESOLVE*]

† $R_{\rm merge} = \sum_{hkl}\sum_i |I_i(hkl) - \langle I(hkl)\rangle|/\sum_{hkl}\sum_i I_i(hkl)$, where $I_i(hkl)$ is the observed intensity and $\langle I(hkl)\rangle$ is the average intensity of symmetry-related observations.

corresponding region in Ecm22 (residues 655–677) resulted in expression of soluble fusion proteins (data not shown). These observations imply that the replacement of variable loop regions by another protein such as T4 lysozyme is generally applicable to other proteins for the construction of stable chimeric proteins.

The Upc2-T4L construct consisted of 438 amino acids including four amino acids from the multiple cloning site of the vector with a molecular weight of 49 235 Da as calculated from the primary sequence. A complete diffraction data set was collected to 2.9 Å resolution for SAD phasing using a selenomethionine-labelled crystal. Data-collection statistics are shown in Table 1. A total of 28 788 measured reflections were collected in the resolution range 50–2.9 Å. Analysis of the diffraction intensities confirmed the space group to be trigonal $P3_1$ or $P3_2$, with unit-cell parameters a = 67.2, b = 67.2, c = 257.5 Å. Strong reflections with indices of 0,0,3n indicated the presence of a screw axis along the c axis. The Matthews coefficient was 3.41 Å^3 Da^{-1} for two copies of Upc2-T4L in the asymmetric unit and 2.27 Å^3 Da^{-1} for three copies in the asymmetric unit, with solvent contents of 63.9 and 45.9%, respectively. A self-rotation function calculated using 9–4 Å resolution data in the κ = 180 and 120° sections showed no dominant features corresponding to a twofold or threefold noncrystallographic symmetry axis (Fig. 4). The observed heights of 4.00σ and 3.53σ for the corresponding self-rotation peaks in the κ = 180° sections are much weaker than the height of 24.41σ for the original peak and do not exceed the heights of all other peaks by twofold. It was not clear whether two or three molecules are in the asymmetric unit based on Matthews coefficients and the self-rotation. We assumed that the high Wilson B factor (80.2 Å^2) of the data set, weak diffraction and fragile crystals might indicate a high solvent content of the crystals corresponding to two molecules in the asymmetric unit. In addition, weak self-rotation peaks might imply that each protomer has sufficiently different conformations probably caused by the hinge motion between Upc2 and T4 lysozyme, which was confirmed by subsequent structure determination.

Molecular replacement using the program *MOLREP* (Vagin & Teplyakov, 2010) with T4 lysozyme as a search model (PDB entry 169l; Zhang *et al.*, 1995) found only one molecule of lysozyme. The top solution with 8.63σ in a rotational search was significantly higher in peak heights than the rest of the other solutions. The second top solution with 4.75σ exceeded the peak heights of ten subsequent solutions by less than 1.2-fold. A search for the second copy of lysozyme was not successful and the MR phasing failed. Therefore, SAD phasing was carried out at 3.0 Å resolution using the program *SOLVE*. The calculations in space group $P3_2$ resulted in good statistics and interpretable electron-density maps. 22 Se sites out of a total of 24 selenomethionines in the Upc-T4L dimer (eight SeMet residues in Upc2 and four in T4L) were found by an automated

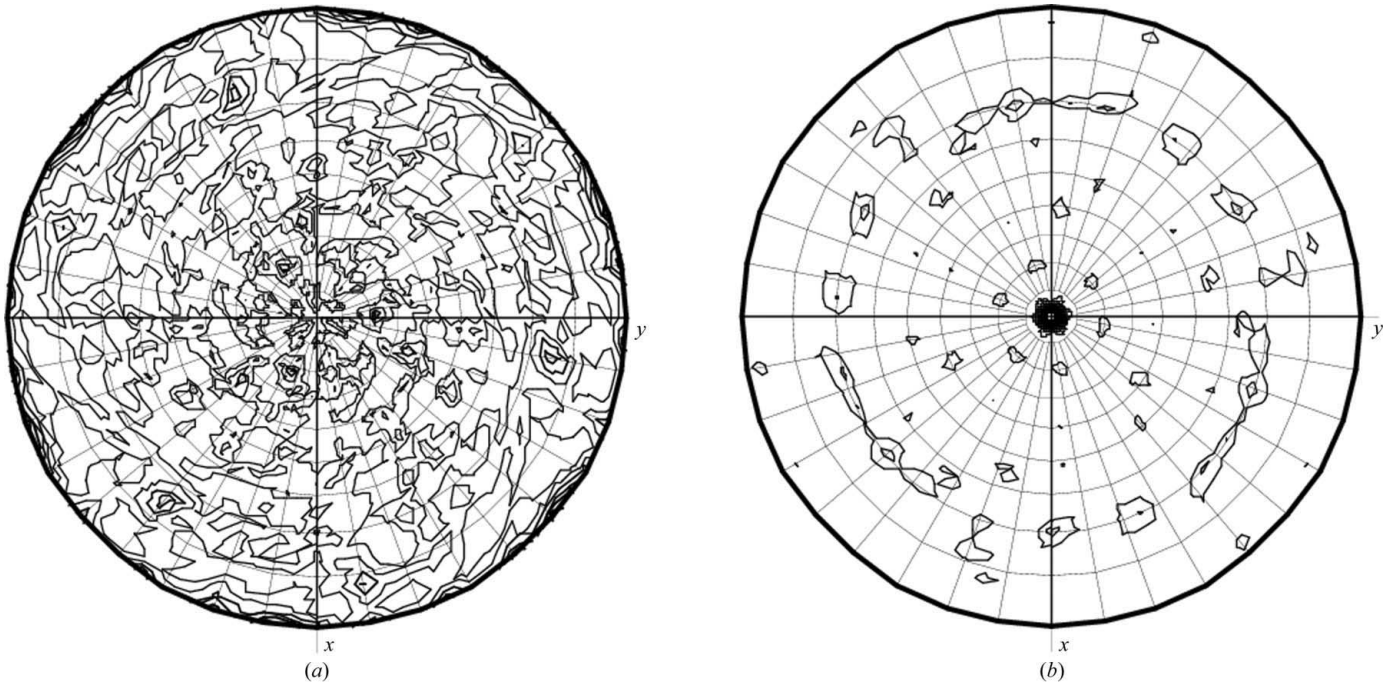

Figure 4
Self-rotation function for Upc2-T4L in the κ = 180° (*a*) and κ = 120° (*b*) sections calculated with *MOLREP* from *CCP4* (Winn *et al.*, 2011) using default parameters, with a search radius of 40.0 Å and data in the resolution range 9.0–4.0 Å.

heavy-atom search with a figure of merit of 0.44 and an overall *Z*-score of 81.1. The other two Se sites in the N-termini of Ucp2 which originate from the multiple cloning site of the expression vector were not found owing to disorder in the crystal. The phases were further improved by density modification using the program *RESOLVE*. The resulting electron-density map with a figure of merit of 0.70 was readily interpretable. Two molecules of Upc2 and one molecule of T4L were clearly visible in the electron-density maps. The second copy of T4L in the asymmetric unit was partially visible in the electron-density map. The N-terminal subdomain of the T4L (residues 15–56) was not visible owing to the disorder caused by the lack of lattice contacts. Two Upc2-T4L protomers have a 12° difference in the hinge angles between Upc2 and T4L, which might have contributed to weak self-rotation peaks. We concluded that the partial disorder in T4L interfered with searching the second copy of lysozyme in the molecular replacement. Model building and structure refinement of the model are currently under way. The forthcoming Upc2 CRD structure will provide key structural information for the understanding of the regulatory mechanism of Upc2.

We would like to thank the beamline staff at AR-NW12A at the Photon Factory. This project was supported by the National Research Foundation of Korea (NRF) (grant No. 2010-0013448) to YJI and the intramural research programme of Chonnam National University to YJI (2011).

References

Chien, E. Y. T., Liu, W., Zhao, Q., Katritch, V., Han, G. W., Hanson, M. A., Shi, L., Newman, A. H., Javitch, J. A., Cherezov, V. & Stevens, R. C. (2010). *Science*, **330**, 1091–1095.
Davies, B. S. J., Wang, H. S. & Rine, J. (2005). *Mol. Cell. Biol.* **25**, 7375–7385.
Doublié, S. (1997). *Methods Enzymol.* **276**, 523–530.
Dunkel, N., Liu, T. T., Barker, K. S., Homayouni, R., Morschhäuser, J. & Rogers, P. D. (2008). *Eukaryot. Cell*, **7**, 1180–1190.
Heilmann, C. J., Schneider, S., Barker, K. S., Rogers, P. D. & Morschhäuser, J. (2010). *Antimicrob. Agents Chemother.* **54**, 353–359.
Hoot, S. J., Smith, A. R., Brown, R. P. & White, T. C. (2011). *Antimicrob. Agents Chemother.* **55**, 940–942.
Lewis, T. L., Keesler, G. A., Fenner, G. P. & Parks, L. W. (1988). *Yeast*, **4**, 93–106.
Otwinowski, Z. & Minor, W. (1997). *Methods Enzymol.* **276**, 307–326.
Rosenbaum, D. M., Cherezov, V., Hanson, M. A., Rasmussen, S. G. F., Thian, F. S., Kobilka, T. S., Choi, H.-J., Yao, X.-J., Weis, W. I., Stevens, R. C. & Kobilka, B. K. (2007). *Science*, **318**, 1266–1273.
Shianna, K. V., Dotson, W. D., Tove, S. & Parks, L. W. (2001). *J. Bacteriol.* **183**, 830–834.
Terwilliger, T. C. (2000). *Acta Cryst.* D**56**, 965–972.
Terwilliger, T. C. & Berendzen, J. (1999). *Acta Cryst.* D**55**, 1872–1877.
Vagin, A. & Teplyakov, A. (2010). *Acta Cryst.* D**66**, 22–25.
Valachovic, M., Bareither, B. M., Shah Alam Bhuiyan, M., Eckstein, J., Barbuch, R., Balderes, D., Wilcox, L., Sturley, S. L., Dickson, R. C. & Bard, M. (2006). *Genetics*, **173**, 1893–1908.
Vik, Å. & Rine, J. (2001). *Mol. Cell. Biol.* **21**, 6395–6405.
Winn, M. D. *et al.* (2011). *Acta Cryst.* D**67**, 235–242.
Zhang, X.-J., Wozniak, J. A. & Matthews, B. W. (1995). *J. Mol. Biol.* **250**, 527–552.
Zhang, Y. & Rao, R. (2010). *Virulence*, **1**, 551–554.